JACS
JOURNAL OF THE AMERICAN CHEMICAL SOCIETY
Article
pubs.acs.org/JACS

Kinetically Controlled Overgrowth of Ag or Au on Pd Nanocrystal Seeds: From Hybrid Dimers to Nonconcentric and Concentric Bimetallic Nanocrystals

Cun Zhu,[†,‡,¶,▽] Jie Zeng,[†,▽] Jing Tao,[§] Matthew C. Johnson,[⊥] Ingeborg Schmidt-Krey,[⊥,∥] Lynn Blubaugh,[■] Yimei Zhu,[§] Zhongze Gu,[‡] and Younan Xia*[,†,¶]

[†]Department of Biomedical Engineering, Washington University, St. Louis, Missouri 63130, United States
[‡]State Key Laboratory of Bioelectronics, School of Chemistry and Chemical Engineering, Southeast University, Nanjing 210096, P.R. China
[§]Condensed Matter Physics and Materials Science Department, Brookhaven National Laboratory, Upton, New York 11973, United States
[⊥]Department of Biology, Georgia Institute of Technology, Atlanta, Georgia 30332, United States
[∥]School of Chemistry and Biochemistry, Georgia Institute of Technology, Atlanta, Georgia 30332, United States
[■]Hitachi High Technologies America, Inc., 944 Clopper Road, Gaithersburg, Maryland 20878, United States

Supporting Information

ABSTRACT: This article describes a systematic study of the nucleation and growth of Ag (and Au) on Pd nanocrystal seeds. By carefully controlling the reaction kinetics, the newly formed Ag atoms could be directed to selectively nucleate and then epitaxially grow on a specific number (ranging from one to six) of the six faces on a cubic Pd seed, leading to the formation of bimetallic nanocrystals with a variety of different structures. In addition to changing the injection rate of precursor, we also systematically investigated other reaction parameters including the capping agent, reductant, and reaction temperature. Our results suggest that the site-selective growth of Ag on cubic Pd seeds could be readily realized by optimizing these reaction parameters. On the basis of the positions of Pd seeds inside the bimetallic nanocrystals as revealed by TEM imaging and elemental mapping, we could identify the exact growth pathways and achieve a clear and thorough understanding of the mechanisms. We have successfully applied the same strategy based on kinetic control to cubic Pd seeds with different sizes and octahedral Pd seeds of one size to generate an array of novel bimetallic nanocrystals with well-controlled structures. With cubic Pd seeds as an example, we have also extended this strategy to the Pd–Au system. We believe this work will provide a promising route to the fabrication of bimetallic nanocrystals with novel structures and properties for applications in plasmonics, catalysis, and other areas.

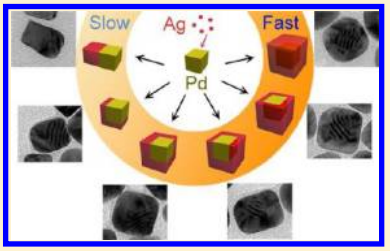

1. INTRODUCTION

Bimetallic nanocrystals have received considerable interest due to their unique properties and potential applications.[1−6] When there is a strong electronic coupling between the two metals, the bimetallic nanocrystals can exhibit greatly enhanced catalytic,[7−12] electronic,[13,14] optical,[15−19] and magnetic properties[20,21] relative to the monometallic components. As a result, recent years have witnessed tremendous efforts devoted to the design, synthesis, and utilization of bimetallic nanocrystals with a variety of compositions, with notable examples including combinations of noble metals such as Au, Ag, Pd, Pt, and Rh.[16−18,22−33]

Among different methods, seed-mediated growth has emerged as one of the most effective routes to the synthesis of bimetallic nanocrystals, by which the size, structure, and morphology of resultant nanocrystals can all be tailored in a more or less controllable fashion.[34−43] In general, seed-mediated growth involves two major steps: (i) synthesis of seeds with uniform and relatively small sizes and (ii) heterogeneous nucleation and growth of another metal on the as-prepared seeds, leading to the formation of bimetallic nanocrystals with desired properties to fit a specific application. By controlling the reaction kinetics of seed-mediated growth, the bimetallic nanocrystals have been successfully prepared with a wide variety of structures.[44−49] However, it still remains a challenge to control the growth mode and thus spatial distribution of the second metal on the surface of a nanocrystal seed. In our previous study, we have shown that three different types of Pd–Ag bimetallic nanocrystals (those with Ag growing on one, three adjacent, and six faces of a Pd seed) could be obtained by manipulating the rate at which $AgNO_3$ precursor was introduced into a reaction system using a syringe pump.[16] However, this method could only be used to manipulate the reaction kinetics within a limited range, and it was very difficult to obtain other structures with Ag growing on two, four, and

Received: June 1, 2012
Published: September 4, 2012

dx.doi.org/10.1021/ja305329g | J. Am. Chem. Soc. 2012, 134, 15822−15831

five faces of a cubic Pd seed. In addition to the injection rate, other parameters such as the capping agent, reductant, and reaction temperature may also influence the reaction kinetics and thus affect the structures of resultant nanocrystals.

Herein, we report a systematic study of the growth mode of Ag on Pd nanocrystal seeds in an effort to control the structures of the resultant Pd−Ag bimetallic nanocrystals. In addition to controlling the rate at which $AgNO_3$ was injected with a syringe pump, we have also systematically evaluated the effects of other reaction parameters such as capping agent, reductant, and reaction temperature. By carefully controlling all these four different parameters, we could deposit Ag on any number (from one to six) of the faces of a cubic Pd seed, leading to the formation of Pd−Ag bimetallic nanocrystals with various novel structures. On the basis of a careful analysis of their TEM images, we also obtained a clear understanding of the spatial distributions of the elements in the resultant bimetallic nanocrystals. Significantly, we were able to identify the growth mode of Ag on Pd seeds according to the positions of the Pd seeds (where Moiré fringes[50] are formed) inside the bimetallic nanocrystals. Furthermore, we also investigated the growth of Ag on other types of Pd seeds, including Pd nanocubes with different sizes and octahedrons of one size. As expected, Ag could also grow on a few or all the faces on these Pd nanocrystal seeds, depending on the reaction conditions involved. These results confirm that the structures of the resultant bimetallic nanocrystals could be conveniently manipulated by controlling the reaction conditions, not only for seeds enclosed by {100} facets but also for those enclosed by {111} facets. In addition, the successful extension of this approach to the Pd−Au system to obtain similarly controllable nanostructures demonstrates its general applicability for the fabrication of bimetallic materials other than Pd−Ag. We believe this work would provide plenty of inspiration and strategies for the fabrication of novel bimetallic materials with well-defined and controllable structures and morphologies for a variety of applications.

2. EXPERIMENTAL SECTION

Chemicals and Materials. Silver nitrate ($AgNO_3$), gold(III) chloride hydrate ($HAuCl_4{\cdot}H_2O$), sodium tetrachloropalladate(II) (Na_2PdCl_4), potassium bromide (KBr), poly(vinyl pyrrolidone) (PVP55 with $M_w \approx 55{,}000$ and PVP10 with $M_w \approx 10{,}000$), L-ascorbic acid (AA), hydrazine (N_2H_4), and sodium hydroxide (NaOH) were all obtained from Sigma-Aldrich. Formaldehyde (HCHO, 37 wt % in H_2O, stabilized with 10−15% methanol) was purchased from Fisher Scientific. Potassium chloride (KCl) was purchased from J.T. Baker. All chemicals were used as received. Deionized water with a resistivity of 18.2 MΩ·cm was used for the preparation of all aqueous solutions.

Synthesis of Pd Nanocubes of 18, 10, and 6 nm in Edge Length. These nanocrystals were prepared by adding an aqueous Na_2PdCl_4 solution into a mixture of AA, PVP, KBr, and KCl aqueous solutions according to our previous report.[51] In a typical synthesis, 8.0 mL of an aqueous solution containing 105 mg of PVP55, 60 mg of AA, and different amounts of KBr and KCl was added to a vial and preheated to 80 °C in air under vigorous magnetic stirring for 10 min. Subsequently, 3.0 mL of an aqueous solution containing 57 mg of Na_2PdCl_4 was injected with a pipet. The reaction lasted for 3 h. The size of Pd nanocubes was controlled by varying the amounts of KBr and KCl, resulting in the formation of Pd nanocubes about 18, 10, and 6 nm in edge length, respectively. The obtained Pd nanocubes were collected by centrifugation, washed three times with deionized water to remove excess PVP and bromide ions, and redispersed in 11 mL of water. TEM images of these Pd nanocubes with different sizes are shown in Figure S1 of the Supporting Information [SI]. Some of the nanocubes were slightly elongated, with an average aspect ratio of 1.2. Since all six faces of the elongated cubes were enclosed by {100} facets, we called the samples "nanocubes" for simplicity.

Synthesis of Pd Octahedrons of 33 nm in Edge Length. Pd octahedrons were prepared by adding 3 mL of an aqueous Na_2PdCl_4 solution (9.5 mg/mL) into 8 mL of an aqueous solution containing 105 mg of PVP55, 0.1 mL of HCHO, and 0.3 mL of the 18-nm Pd nanocubes at 60 °C under magnetic stirring.[52] The vial was removed from the oil bath 3 h later. After collection by centrifugation and washing three times with water, the product was redispersed in 11 mL of water.

Synthesis of Pd−Ag Bimetallic Nanocrystals with Controlled Structures. Typically, 4.6 mL of an aqueous solution containing the as-prepared 18-nm Pd nanocubes (0.35 mM in terms of elemental Pd), AA (5.7 mM), PVP (PVP10 or PVP55), and NaOH at specific concentrations was added to a 20-mL vial. The mixture was held at a designated temperature for 20 min under magnetic stirring. Meanwhile, 1.1 mL of an aqueous $AgNO_3$ solution (3.6 mM) was freshly prepared at room temperature and injected into the vial at a controlled rate. In all these cases, the solution was stirred for another 2 min after injection to allow the reaction to complete. The product was collected by centrifugation at 12,000 rpm for 15 min and washed with water three times. Table 1 shows the exact values for the concentration and molecular weight of PVP, the concentration of NaOH, the injection rate for $AgNO_3$ solution, and the reaction temperature associated with each synthesis.

Table 1. Reaction Conditions for the Synthesis of Pd−Ag Bimetallic Nanocrystals with Different Structures When 18-nm Pd Cubes Were Used As the Seeds

N[a]	capping agent	[PVP][b] (mM)	[NaOH] (mM)	R_{AgNO_3}[c] (mL/h)	T (°C)	results (Figure)
1	PVP10	156.7	0	1.0	0	1A, 6D
2	PVP10	156.7	0	1.0	20	6E
	PVP10	156.7	0	30	20	1B, 6A
3	PVP10	156.7	3.4	30	20	6B
	PVP10	156.7	0	1.0	60	1C, 6F
	PVP10	156.7	3.4	one-shot	60	5A
4	PVP10	156.7	5.7	30	20	6C
	PVP10	39.2	3.4	one-shot	60	1D, 5B
5	PVP10	27.4	3.4	one-shot	60	1E, 5C
6	PVP10	19.6	3.4	one-shot	60	1F, 5D
	PVP55	39.2	3.4	one-shot	60	S6 (SI)

[a]N: number of faces for Ag to grow on a Pd cube. [b]The concentration of PVP was calculated in terms of the repeating unit with a molecular weight of 111 g/mol. [c]Injection rate of $AgNO_3$.

For the growth of Ag on 10- and 6-nm Pd nanocubes and 33-nm Pd octahedrons, we used the same procedure as described for the 18-nm Pd nanocubes. The detailed experimental conditions can be found in Table 2 and SI, Table S1.

Table 2. Reaction Conditions for the Synthesis of Pd−Ag Bimetallic Nanocrystals with Different Structures When 33-nm Pd Octahedrons Were Used As the Seeds

N[a]	capping agent	[PVP][b] (mM)	[NaOH] (mM)	R_{AgNO_3}[c] (mL/h)	T (°C)	results (Figure)
1−2	PVP10	19.6	0	1.5	0	7B
4−5	PVP10	19.6	3.4	30	20	7C
8	PVP55	2.0	5.7	one-shot	60	7D

[a]N: number of faces for Ag to grow on a Pd octahedron. [b]The concentration of PVP was calculated in terms of the repeating unit with a molecular weight of 111 g/mol. [c]Injection rate of $AgNO_3$.

Synthesis of Pd–Au Bimetallic Nanocrystals with Controlled Structures. Typically, 4.6 mL of an aqueous solution containing the as-prepared 18-nm Pd nanocubes (0.35 mM in terms of elemental Pd), AA (5.7 mM), KBr (43.5 μM), and PVP55 (3.9 mM) was added to a 20 mL vial. The mixture was held at room temperature for 20 min under magnetic stirring. Meanwhile, a 0.6 mM aqueous $HAuCl_4$ solution was prepared at room temperature. For the synthesis of Pd–Au hybrid dimers and eccentric nanocrystals, the aqueous $HAuCl_4$ solution was injected into the vials using a syringe pump at rates of 0.5 mL/h and 5.0 mL/h, respectively. For the synthesis of Pd@Au core–shell nanocrystals, a specific amount of the aqueous $HAuCl_4$ solution was quickly added into the vial using a pipet. In all cases, the solution was maintained with stirring for another 2 min after injection to allow the reaction to complete. The product was collected by centrifugation at 12,000 rpm for 15 min and washed with water three times.

Instrumentation. Transmission electron microscopy (TEM) images were taken using a Tecnai G2 Spirit Twin microscope (FEI, Hillsboro, OR), an HT7700 microscope (Hitachi, Tokyo, Japan), or a JEM-1400 microscope (JEOL, Tokyo, Japan). All the microscopes were operated at 120 kV. High-resolution TEM (HRTEM), scanning TEM, energy dispersive X-ray (EDX) mapping, and EDX analyses were performed using a JEOL 2100F microscope operated at 200 kV. The concentration of elemental Pd was determined using a Perkin-Elmer Elan DRC II inductively coupled plasma mass spectrometry (ICP-MS). The samples for ICP-MS were prepared by dissolving 10 μL of the suspension of Pd nanocrystals with 30 μL of concentrated HNO_3. The resultant solution was further diluted to a level of 100 ppb for ICP-MS analysis. Extinction spectra of all the Pd–Ag nanocrystals were recorded using a UV–vis spectrometer (Varian, Cary 50).

3. RESULTS AND DISCUSSION

Structural Analysis of Pd–Ag Bimetallic Nanocrystals with Ag Grown on Different Numbers of Faces of a Pd Cube. We chose Pd nanocubes (18 nm in size, shown in SI, Figure S1) as the seeds because this type of nanostructure provides a model system with six {100} faces on the surface. Each one of these faces could act as a nucleation site for the newly formed Ag atoms. We conducted the seed-mediated growth by using a syringe pump to inject an aqueous $AgNO_3$ solution into a system containing the Pd seeds, AA, and PVP. By adjusting the injection rate and other reaction parameters, such as the capping agent, reductant, and reaction temperature (see Table 1 for details), we were able to precisely control the growth mode of Ag on Pd in terms of how many faces of a cubic Pd seed were involved in the nucleation and growth of Ag. The structures of resultant Pd–Ag bimetallic nanocrystals and spatial distributions of their elements were determined by TEM. Figure 1, A–F, shows representative TEM images of the six distinct types of Pd–Ag bimetallic nanocrystals with Ag being selectively deposited on one, two adjacent, three adjacent, four, five, and six faces of a cubic Pd seed, respectivley. When Pd cubes of 10 and 6 nm in edge length were employed as the seeds, similar structures were also observed, as shown in SI, Figure S2.

Due to the existence of a misfit between the crystal lattices of Ag and Pd, alternative dark and bright patterns (known as Moiré fringes) were clearly observed in the region where Pd and Ag overlapped. These fringes serve as an obvious mark for pinpointing the position of Pd seed in a bimetallic nanocrystal. Consequently, the growth mode of Ag on Pd seeds could be classified according to the positions of Pd seeds in the bimetallic nanocrystals. For example, when Ag atoms grew from three adjacent faces of a Pd seed, Moiré fringes would only be observed at one of the corners of a bimetallic nanocrystal (see the inset of Figure 1C). When Ag atoms grew on one, two, four, and five faces, we had to consider different orientations of

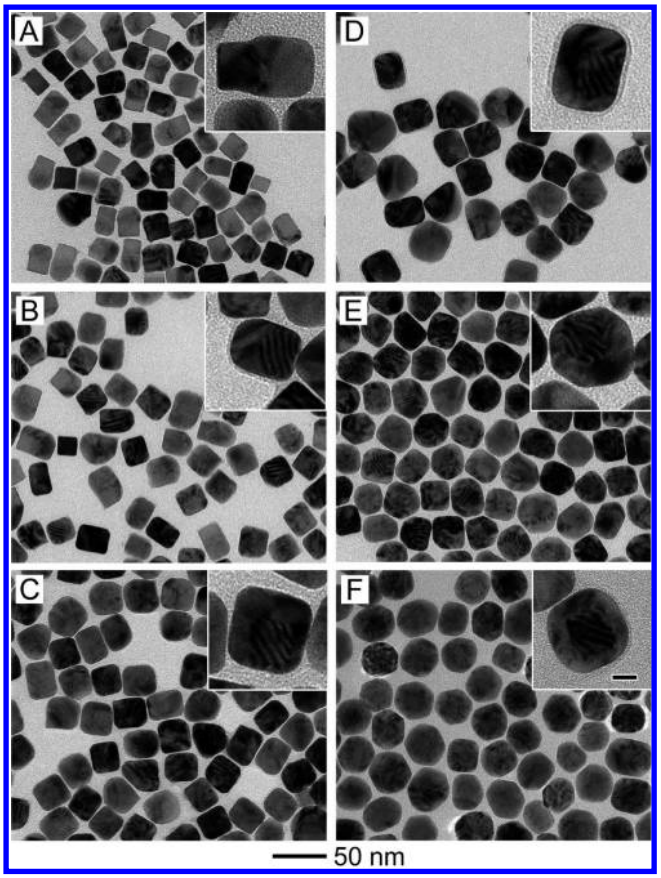

Figure 1. TEM images of six different types of Pd–Ag bimetallic nanocrystals obtained from the seed-mediated growth of Ag on 18-nm Pd cubes under various conditions specified in Table 1. The deposition of Ag was confined to (A) one, (B) two, (C) three, (D) four, (E) five, and (F) six faces of a cubic Pd seed. The scale bar in the inset of (F) is 10 nm and applies to all other insets.

the bimetallic nanocrystals relative to the electron beam during TEM imaging. Figure 2 shows a schematic that illustrates all major growth modes we have observed for the Pd–Ag system, together with the corresponding TEM images viewed along different directions. By carefully analyzing a large number of particles in the TEM image of a sample, we were able to identify the exact growth pathway.

When Ag was grown on three adjacent faces of a cubic Pd seed to yield a nonconcentric Pd–Ag cube or all six faces to form a concentric Pd@Ag core–shell cube, the products only gave one projected structure, regardless of their orientations relative to the electron beam. In the former case, the Pd seed occupied one of the corners of a nonconcentric cube. Therefore, only this corner displayed Moiré fringes over the area corresponding to the Pd seed (Figure 2, III-A). For the latter case, the Pd seed was located in the center of a bimetallic nanocrystal, where Moiré fringes were observed (Figure 2, VI-A).

For Pd–Ag dimers with Ag grown on only one of the six faces of a cubic Pd seed, there were two different structures observed under TEM. When the Pd–Ag interface was parallel to the electron beam, the Pd seed was located on one side of the hybrid structure while the Ag portion was located on the other side. No Moiré fringes would be observed, as shown in Figure 2, I-A (viewing along the I-A direction). When the Pd–Ag interface was perpendicular to the electron beam, Moiré

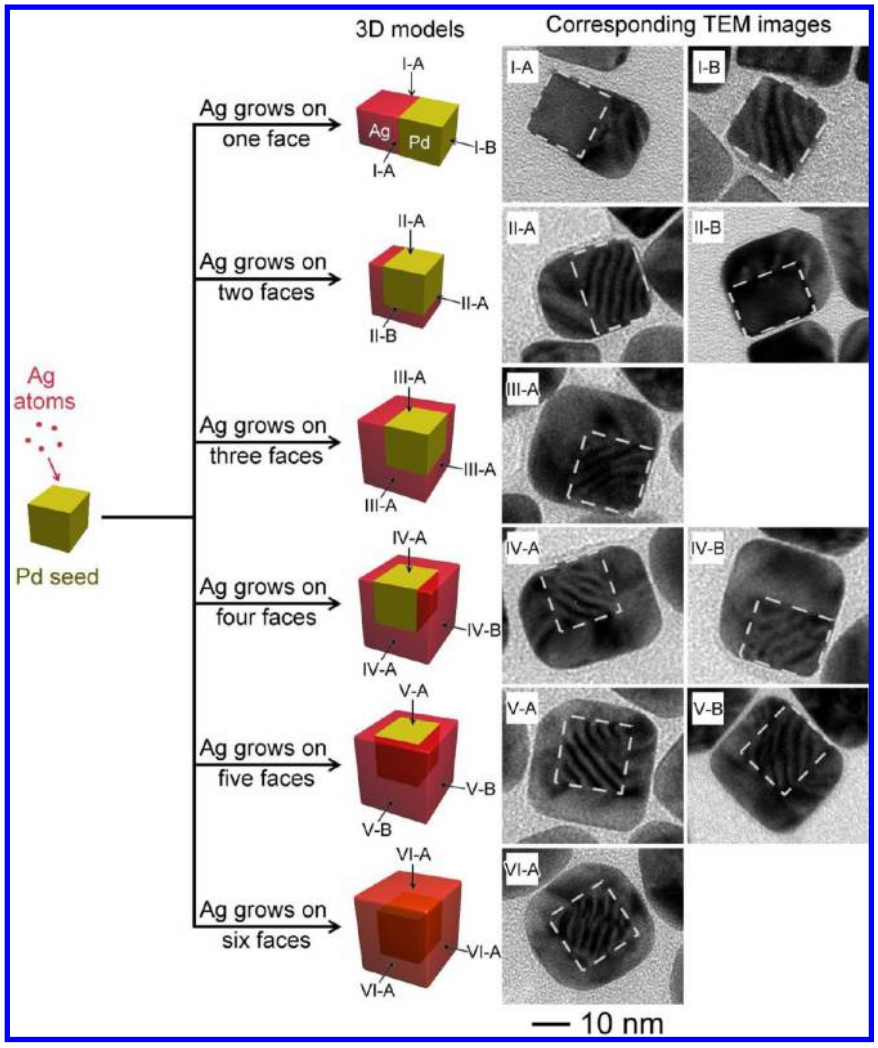

Figure 2. Schematic illustration showing the growth Ag on different numbers of the faces of a cubic Pd seed and their corresponding TEM images viewed along different directions. The possible viewing directions are marked in the 3D models and are also shown on the upper-left corner of each TEM image. The white lines in the TEM images roughly indicate the position of the cubic Pd seeds. The scale bar applies to all the TEM images.

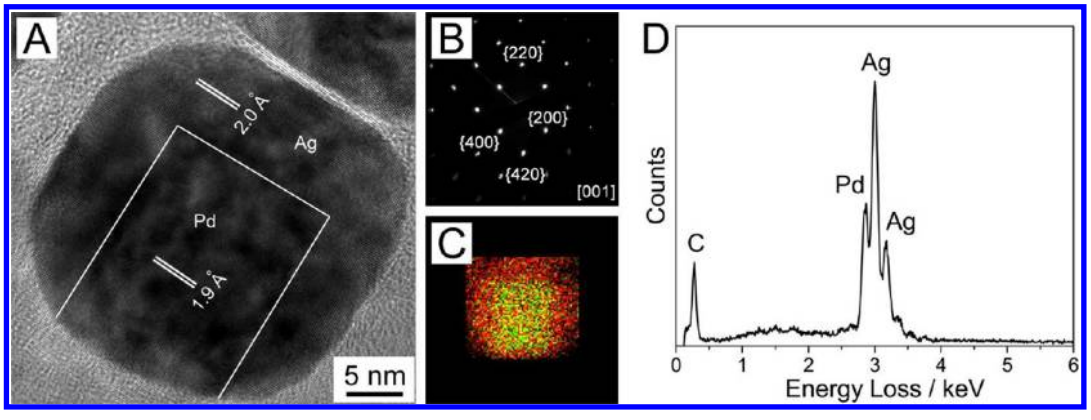

Figure 3. Structural analysis of a Pd–Ag bimetallic nanocrystal with the Pd cube located close to one of the six faces. (A) HRTEM image, (B) SAED pattern, (C) EDX mapping image, and (D) EDX pattern of this particle. For HRTEM image, the white lines roughly indicate the boundary between the Ag portion and the Pd seed. For EDX mapping, Pd atoms are shown in green, while Ag atoms are shown in orange.

fringes were observed to cover the entire particle, as shown in Figure 2, I–B (viewing along the I–B direction). Similarly, when Ag was grown on two, four, or five faces of a cubic Pd seed, the TEM images could show two distinct structures, depending on the viewing directions (see Figure 2 for a detailed analysis).

We further characterized the sample in Figure 1E using HRTEM and EDX microanalysis. Figure 3A shows a typical HRTEM image of an individual particle along the [001] zone

dx.doi.org/10.1021/ja305329g | J. Am. Chem. Soc. 2012, 134, 15822–15831

axis. It was found that the lattice fringes were coherently extended from the Pd core to the Ag portion, suggesting an epitaxial relationship between these two metals. The {200} fringes in the Pd and Ag regions showed periods of 1.9 and 2.0 Å, respectively, consistent with the face-centered cubic (*fcc*) Pd and Ag. The selected area electron diffraction (SAED) pattern recorded from the particle also showed a single-crystal structure for both Pd and Ag components, as shown in Figure 3B. Minor splitting could be observed for each diffraction spot due to the relatively large mismatch (4.5%) in lattice constant between these two metals. The distributions of Pd and Ag were clearly resolved by EDX elemental mapping (Figure 3C), supporting the formation of Pd–Ag bimetallic nanocrystals with Ag grown on five of the six faces of a cubic Pd seed. The corresponding EDX spectrum (Figure 3D) also supported our analysis. It should be pointed out that the positions of the Pd seeds could be difficult to resolve in some of the Pd–Ag bimetallic nanocrystals. In order to obtain a better understanding of their structures as well as the growth modes, we have extensively characterized three representative Pd–Ag bimetallic nanocrystals with Ag epitaxially grown on one, three adjacent, and five faces of the Pd seeds by recording TEM images at different tilt angles (SI, Figures S3 and S4). Depending on the orientations of the Pd–Ag bimetallic nanocrystals, the Pd seeds could only be identified at certain tilt angles when the Moiré fringes were clearly observed due to the low contrast between Pd and Ag components. These results also suggest that the products of a synthesis were dominated by Pd–Ag bimetallic nanocrystals evolving through one specific growth pathway.

It is worth pointing out that, besides the structures shown in Figure 2, other structures might be obtained when Ag was grown on two, three, or four of the six faces of a cubic Pd seed. For example, Ag might grow on two opposite faces, two opposite faces and one other face, or two pairs of opposite faces of a cubic Pd seed (see SI, Figure S5). In reality, these growth modes were rarely observed in the Pd–Ag system. The exact reason is still not clear at the moment, but it might be related to the collision pattern of the Ag atoms with a Pd seed, as well as the surface diffusion of Ag adatoms.[53−55]

Formation Mechanisms of the Pd–Ag Bimetallic Nanocrystals with Different Structures. We believe the collision of newly formed Ag atoms with a Pd surface is mainly responsible for the deposition of Ag on selected faces of the Pd seeds and thus the formation of Pd–Ag bimetallic nanocrystals with different structures. Faster reduction of Ag precursor would generate a larger number of Ag atoms at any moment to interact with the Pd surface during the nucleation stage, thus promoting the collision of Ag atoms with a larger number of Pd faces to form active growth sites. Once the growth sites are formed, the subsequently formed Ag atoms preferred to deposit on these sites, rather than forming new sites on other faces due to the relatively large lattice mismatch between Pd and Ag. As a result, the formation of active growth sites on selected Pd faces during the nucleation stage plays a critical role in determining the deposition of Ag atoms and thus the growth mode. Significantly, the initial collision and nucleation can be manipulated by controlling the reaction kinetics.[16] Besides the pattern of collision, surface diffusion of Ag adatoms might also contribute to the formation of active growth sites. Although deposition of Ag atoms on the edges or vertices of a Pd seed is also possible, the deposited Ag atoms could rapidly diffuse to adjacent faces in an effort to reduce the surface energy. In a sense, the formation of Pd–Ag bimetallic nanocrystals with Ag selectively grown on two or three faces of the Pd seeds was probably caused by the diffusion of Ag atoms from one edge or vertex to two or three adjacent faces, thus generating active growth sites on these faces to direct the subsequent deposition and growth of Ag. The Ag adatoms also have the possibility to diffuse from one face to adjacent faces, but it should be much more difficult than the "edge-to-face" or "vertex-to-face" diffusion paths owing to the relatively large energy barrier involved.

Optical Properties of the Pd–Ag Bimetallic Nanocrystals. Figure 4 shows the extinction spectra recorded from aqueous suspensions of the as-prepared Pd–Ag bimetallic nanocrystals with Ag grown on different numbers of faces of cubic Pd seeds. For the Pd–Ag dimeric nanocrystals where Ag only grew on one of the six faces of a Pd seed, the major localized surface plasmon resonance (LSPR) peak was located at 421 nm. For those with Ag deposited on two, three, four, and five faces, the LSPR peaks increasingly blue-shifted to the region between 415 and 400 nm along with an increase in the number of faces being covered by Ag. For the Pd@Ag concentric core–shell nanocrystals where Ag was deposited on all the six faces, the peak appeared at an even shorter wavelength of ~375 nm. In principle, the size (or volume) of the Ag component, the geometric shape of the Ag component, and the electron transfer between the Pd and Ag components could all affect the LSPR properties of the Pd–Ag bimetallic nanocrystals. Our analysis suggested that the electron transfer between the Pd and Ag components was mainly responsible for the continuous blue shift, in which the electron density of the Ag component was increased due to electron transfer from Pd to Ag because Pd is more electronegative than Ag and has higher red/ox potential (The reduction potential of Pd^{2+}/Pd is 0.91 V versus RHE, while that of Ag^{+}/Ag is 0.80 V versus RHE).[56−61] More electrons would be transferred from Pd to Ag when more faces of the Pd seed were covered by Ag, leading to a more significant blue-shift for the LSPR peak. Interestingly, the shoulder peak at ~350 nm that has been proven to originate from the Pd–Ag interface[16] did not show any apparent shift in peak position, whereas its intensity increased along with the increase in the number of faces involved in growth.

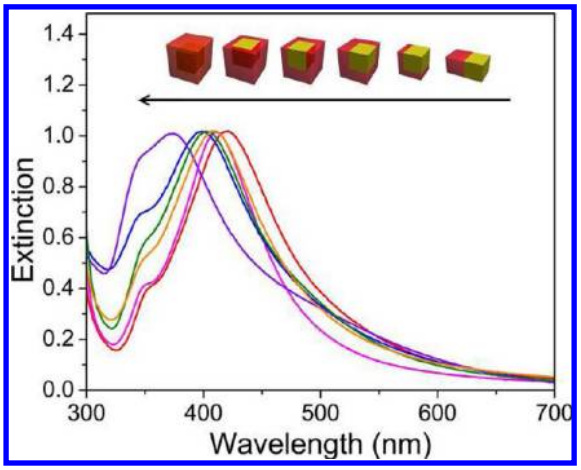

Figure 4. Extinction spectra of the as-obtained Pd–Ag bimetallic nanocrystals with Ag growing on different numbers of the faces of a cubic Pd seed. The major LSPR peak blue-shifted along with the increase in the number of faces involved in the growth.

dx.doi.org/10.1021/ja305329g | J. Am. Chem. Soc. 2012, 134, 15822−15831

The Effect of Capping Agent on the Growth Mode of Ag. To screen the conditions under which various types of Pd−Ag bimetallic nanocrystals were obtained, we systematically studied the effects of different reaction parameters on the growth mode of Ag on Pd seeds. We initially focused on the capping agent, with regard to the concentration and molecular weight of PVP. To this end, we conducted experiments with Pd nanocubes of 18 nm in edge length as the seeds and PVP10 of various molar concentrations as the capping agent. Here the concentration of PVP was calculated in terms of the repeating unit of PVP with a molecular weight of 111 g/mol. The concentration of PVP10 in the solution was first set to 156.7 mM. After deposition of Ag, we found that the Pd cubes were mainly located at the corners of resultant particles (see Figure 5A), indicating the formation of Pd−Ag bimetallic nanocrystals with Ag grown on three adjacent faces of the Pd seed. Reducing the amount of PVP10 to 39.2, 27.4, and 19.6 mM caused the Ag to grow on four, five, and six faces of the Pd seed, respectively, as shown in B−D of Figure 5. We believe that when the concentration of PVP was reduced, the coverage density of PVP chains on the surfaces of the Pd seeds or the growing Pd−Ag bimetallic nanocrystals would drop.[62] This would increase the probability for the newly formed Ag atoms to collide with a larger number of Pd faces, leading to the formation of Pd−Ag bimetallic nanocrystals with Ag growing on more faces of a seed. At the same time, more noncubic Pd−Ag bimetallic nanocrystals would form as the concentration of PVP was reduced. By carefully analyzing their structures, we found that these noncubic nanocrystals were still formed through a mechanism or growth mode similar to that of the cubic Pd−Ag nanocrystals. As the size of the Ag components increased and the concentration of PVP in the solution was reduced during a synthesis, the capping efficiency of PVP for the Ag(100) surface of the Pd−Ag nanocrystals would drop, resulting in the formation of noncubic Pd−Ag bimetallic nanocrystals.[62] In addition, the increase in surface energy as induced by strain due to the relatively large mismatch in lattice constant between Pd and Ag might also contribute to the formation of a noncubic shape.

We also investigated the effect of molecular weight of PVP on the growth mode of Ag. The experiment was conducted by simply changing PVP10 to PVP55 and keeping other conditions the same. The concentration of PVP55 was also set to 39.2 mM in terms of repeating unit, just the same as that of PVP10 used for the sample shown in Figure 5B. In comparison with PVP10, PVP55 tended to generate Pd−Ag bimetallic nanocrystals with Ag grown on more (in this case, six) faces of the seed (SI, Figure S6). This difference might be caused by the larger size and thus stronger steric effect of PVP55 that made the formation of Ag^+-PVP55 complex more difficult than that of Ag^+-PVP10.[62] In this case, Ag preferred to nucleate and grow on more faces of the Pd seed.

The Effect of Reductant. We also investigated the role of reductant in the formation of Pd−Ag bimetallic nanocrystals. It was reported that the reducing power of AA was dependent on the pH value and would be enhanced with the introduction of more NaOH.[63] As such, we could manipulate the reaction kinetics by varying the concentration of NaOH in an effort to generate different types of Pd−Ag bimetallic nanocrystals. Figure 6, A−C, shows the outcomes for the reaction conditions summarized in Table 1. In the absence of NaOH, the products were dominated by nanocrystals with Ag grown on two faces of a Pd seed (Figure 6A). At a relatively low concentration of NaOH (3.4 mM), we observed Ag grown on three faces of the Pd seed (Figure 6B). At a relatively high concentration of NaOH (5.7 mM), Ag preferred to grow on four faces of the Pd seed (Figure 6C). The structures observed correlated well with the reaction kinetics. As expected, a relatively low concentration of NaOH corresponded to slow reduction from Ag^+ to Ag^0, which only produced a small quantity of Ag atoms in the solution. The scarce supply of Ag atoms would promote growth of Ag on only a few faces of the Pd seed. In contrast, the high concentration of NaOH made AA a rather strong reducing agent, greatly accelerating the reaction and shifting the growth toward a more isotropic mode. As a result, Ag tended to grow on more faces of the Pd seed.

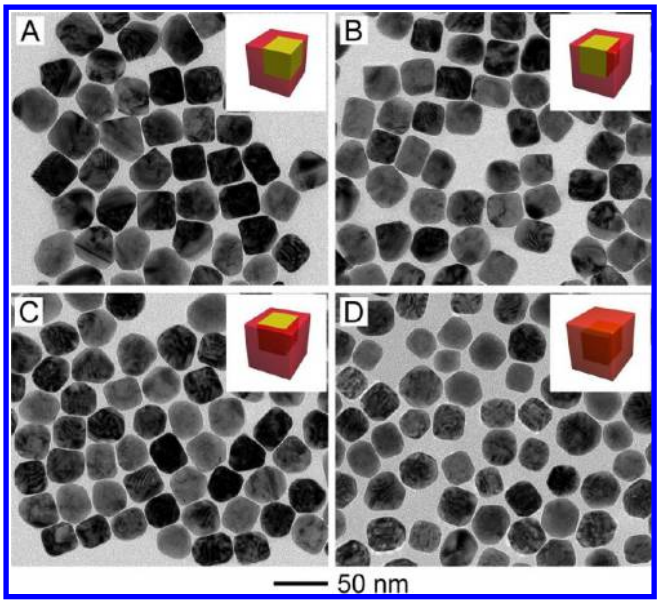

Figure 5. TEM images of Pd−Ag bimetallic nanocrystals grown from 18-nm Pd nanocubes in the presence of (A) 156.7, (B) 39.2, (C) 27.4, and (D) 19.6 mM PVP10 as the capping agent. The insets show the corresponding 3D model for each type of the product.

To confirm the role played by the reductant in controlling the growth mode for Ag and thus the structure of resultant Pd−Ag bimetallic nanocrystals, we also conducted two experiments by replacing AA with a weaker reductant (formaldehyde) and a stronger reductant (hydrazine).[64] Other reaction conditions such as the capping agent (156.7 mM of PVP10), and the concentration of NaOH (0 mM), the injection rate (30 mL/h) for $AgNO_3$ solution, and the reaction temperature were all kept the same as those used for the sample shown in Figure 1B. As expected, the products showed completely different structures compared with that when AA was used as the reductant (in this case, Ag grew on two faces of a Pd seed, see Figure 1B); formaldehyde favored the deposition of Ag on only one of the faces of a Pd seed (SI, Figure S7A), while hydrazine led to the deposition of Ag on all six faces (SI, Figure S7B). The difference in structure is believed to arise from the difference in reaction kinetics associated with the reducing agents.

The Effect of Reaction Temperature. Besides control of the capping agent and the reductant, we also tried to modulate the reaction kinetics by tuning the reaction temperature. The results are shown in Figure 6, D−F. It was found that Ag mainly grew on only one face of the Pd seed when the reaction was performed in an ice-bath (Figure 6D). When the reaction temperature increased to room temperature and 60 °C, Ag

dx.doi.org/10.1021/ja305329g | J. Am. Chem. Soc. 2012, 134, 15822−15831

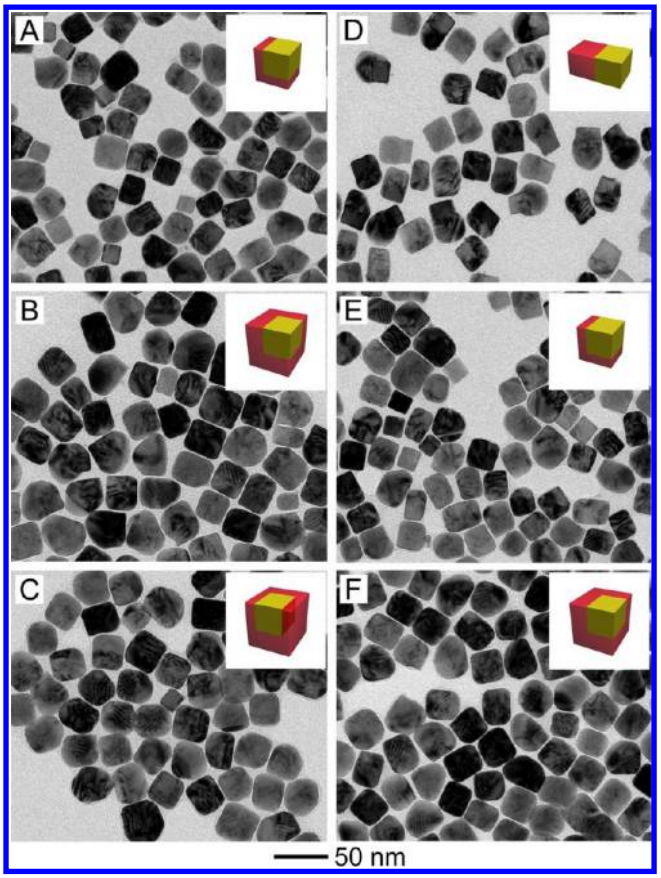

Figure 6. TEM images of Pd−Ag bimetallic nanocrystals grown from 18-nm Pd nanocubes under different conditions. For (A−C), the syntheses were conducted in the presence of (A) 0, (B) 3.4, and (C) 5.7 mM NaOH, respectively, at room temperature. For (D−F), the syntheses were conducted in the absence of NaOH at (D) 0 °C (in an ice-bath), (E) 20 °C (room temperature), and (F) 60 °C, respectively. The inset shows the corresponding 3D model for each type of structure.

preferred to grow on two and three faces of the Pd seed, respectively (Figure 6, E and F). In general, the increase of reaction temperature would effectively accelerate the reduction from Ag^+ to Ag^0, leading to the increase of the concentration of Ag atoms in the solution and thus the enhancement of collision frequency of the Pd seed with Ag atoms. As such, it is not difficult to understand that reaction at an elevated temperature would facilitate nucleation and growth of Ag on more faces of a Pd seed.

Use of Pd Octahedrons as the Seeds. We then extended this approach to controlling the structure of Pd−Ag bimetallic nanocrystals involving Pd octahedrons enclosed by {111} facets as the seeds. Figure 7A shows a TEM image of the as-prepared octahedral Pd seeds with an edge length around 33 nm. Although the facets of Pd octahedrons are completely different from those of Pd cubes, it was still feasible to control the growth mode and thus spatial distribution of Ag on an octahedral Pd seed. We conducted the growth under three distinct sets of parameters, as shown in Table 2. The first set of experiments was to control the reaction at a slow rate. In this case, we obtained Pd−Ag dimeric nanocrystals with Ag growing on only one or two {111} faces of the octahedral Pd seed (Figure 7B). The second set of experiments was expected to speed up the reaction, which produced Pd−Ag nonconcentric nanocrystals with Ag growing on four or five faces of the seed (Figure 7C). The third set of experiments was designed to boost the reaction rate up to a relatively high level. As expected, Pd@Ag core−shell nanocrystals with Ag growing on all the eight faces of an octahedral Pd seed were obtained (Figure 7D). It can be concluded that the reactions conducted at a faster reduction of the Ag precursor would favor the nucleation and growth of Ag on more faces of a Pd seed. These results confirmed that the strategy based on kinetic control could be extended to seeds with different shapes.

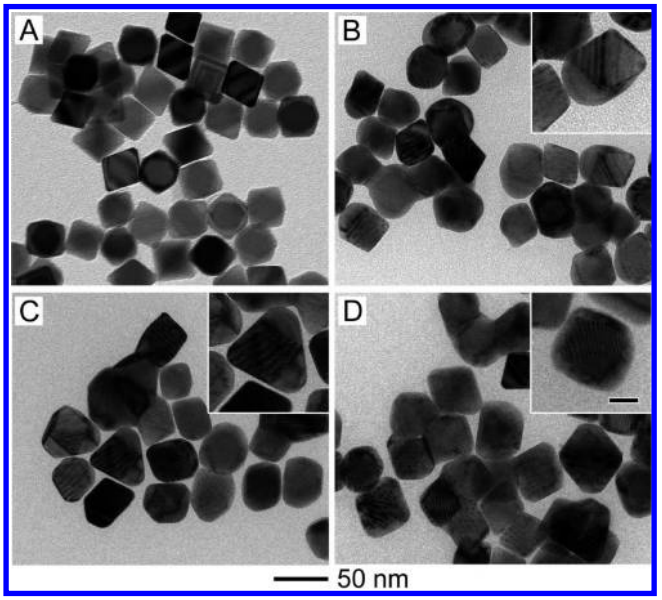

Figure 7. TEM images of (A) 33-nm octahedral Pd seeds and (B−D) Pd−Ag bimetallic nanocrystals grown from the octahedral seeds under different conditions specified in Table 2. The scale bar in the inset of (D) indicates 20 nm and applies to all other insets.

Control of the Growth Mode of Au on Pd Cubes. In a preliminary study, we also extended this synthetic approach to other bimetallic systems such as Pd−Au to demonstrate its versatility in controlling the structural evolution of a seed-mediated growth process. The experiments were conducted at room temperature with 18-nm Pd cubes as the seeds to direct the growth of Au in the presence of PVP55 as a capping agent, AA as a reductant, and $HAuCl_4$ as a precursor. By manipulating the rate at which the $HAuCl_4$ precursor was introduced, the resultant Au atoms could also be directed to deposit on one, three (approximately), and six faces of a cubic Pd seed, generating Pd−Au hybrid dimers (Figure 8, A−C), Pd−Au nonconcentric nanocrystals (Figure 8, D−F), and Pd@Au core−shell nanocrystals (Figure 8, G−I), respectively. This set of experiments clearly demonstrated that it was the reaction kinetics rather than the specific combination of metals that was responsible for the site-selective deposition, suggesting that the kinetic control could be extended to other combinations of metals as well. Interestingly, besides the common growth modes schematically illustrated in Figure 2, we also observed other modes (like those shown in SI, Figure S5) in the Pd−Au system. The corresponding TEM images are shown in SI, Figure S8. In these cases, the Au atoms could nucleate and then grow on one or two pairs of opposite faces of a cubic Pd seed other than on adjacent faces. These new growth modes were hardly observed in the Pd−Ag system. This difference might be

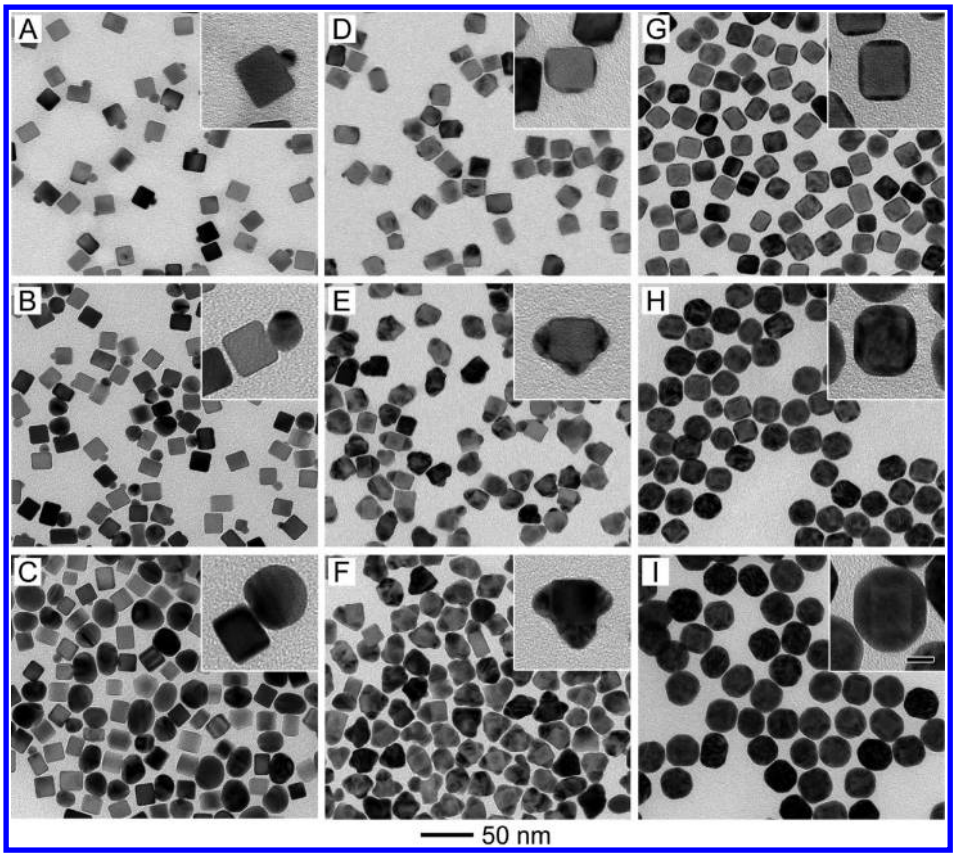

Figure 8. Three different types of Pd−Au bimetallic nanocrystals obtained by controlling the injection rate of $HAuCl_4$ into cubic Pd seeds. (A−C) TEM images of Pd−Au dimers obtained by injecting the $HAuCl_4$ solution at 0.5 mL/h, and the total volumes of added $HAuCl_4$ solution were: (A) 0.7, (B) 1.4, and (C) 2.5 mL. (D−F) TEM images of Pd−Au eccentric nanocrystals obtained by injecting the $HAuCl_4$ solution at 5.0 mL/h, and the total volumes of added $HAuCl_4$ solution were: (D) 0.8, (E) 2.0, and (F) 3.4 mL. (G−I) TEM images of Pd@Au core−shell nanocrystals obtained by adding all of the $HAuCl_4$ solution at one shot with a pipet, and the total volumes of added $HAuCl_4$ solution were: (G) 1.3, (H) 2.8, and (I) 4.5 mL. The scale bar in the inset of (I) is 10 nm and applies to all other insets.

caused by the slow mobility of Au atoms relative to Ag atoms, which could prevent the Au atoms randomly nucleated on different faces of a Pd seed in the early stagy from migrating to other faces. As such, it is not difficult to understand that Au atoms could be deposited on any combination of faces on the surface of a Pd seed (not just the adjacent faces but also faces in opposite positions), providing more variations in growth mode relative to the Pd−Ag system. It is worth pointing out that, for all cases, the Pd seeds retained their original size and shape, indicating that they were intact during the overgrowth of Ag or Au.

4. CONCLUSION

In summary, we have systematically studied the nucleation and growth of Ag and Au on Pd nanocrystals to generate bimetallic nanocrystals with well-defined and controllable structures. By controlling the reaction kinetics, Ag could be directed to selectively nucleate and then grow on any number of faces of a cubic Pd seed, ranging from only one face to generate Pd−Ag hybrid dimeric structures to as many as all six faces to form Pd@Ag concentric core−shell nanocrystals. On the basis of the positions of the Pd seeds (where Moiré fringes appeared) and their TEM images projected along different directions, it was feasible to identify the growth modes for the different bimetallic nanocrystals. In addition to the injection rate of the $AgNO_3$ precursor that has been reported previously, other reaction conditions including the concentration and molecular weight of the PVP capping agent, pH value, reducing agent, and reaction temperature all contributed to the reaction kinetics. We thus systematically investigated their effects on the growth mode of Ag on Pd. It was demonstrated that Ag would grow on more faces of a Pd seed under the circumstances of a lower concentration and higher molecular weight of PVP, a stronger reductant, and higher temperature, indicating that faster reaction rate would be beneficial for Ag to grow on more faces of the seed. By conducting selective growth of Ag on octahedral Pd seeds, we proved that the control of reaction kinetics could be applied not only to seeds enclosed by {100} facets but also to seeds enclosed by {111} facets. We further extended this approach to the Pd−Au system.

This work provides a versatile approach to the fabrication of bimetallic nanocrystals with well-controlled spatial distributions for the constituent elements. The new types of bimetallic nanocrystals are attractive for applications in photonics as they displayed tunable LSPR properties. We also believe that this strategy for engineering the spatial distributions of elements in a bimetallic nanocrystal offers a novel and reliable approach to the fabrication of plasmonic nanostructures with enhanced sensing and surface-enhanced Raman scattering (SERS) capabilities. In addition, these novel bimetallic nanocrystals might find use in catalysis due to the well-controlled spatial distributions of different elements.

dx.doi.org/10.1021/ja305329g | J. Am. Chem. Soc. 2012, 134, 15822−15831

■ ASSOCIATED CONTENT

Supporting Information

TEM images of Pd cubes with average edge lengths of 18 nm, 10 nm, and 6 nm, respectively, which served as seeds for the growth of Ag; TEM images of Pd−Ag bimetallic nanocrystals with different structures obtained from Pd cubes of 10 and 6 nm in edge length; a schematic illustration of other possible growth modes based on the deposition of Ag on two, three, or four of the faces of a cubic Pd seed; TEM image of Pd−Ag hybrid nanocrystals with a core−shell structure synthesized in the presence of 39.2 mM PVP55 as the capping agent; TEM images of Pd−Ag hybrid nanocrystals obtained using different reductants; TEM images of Pd−Au hybrid nanocrystals with Au being deposited on opposite faces of a cubic Pd seed rather than adjacent faces; and TEM images recorded at different tilt angles. This material is available free of charge via the Internet at http://pubs.acs.org.

■ AUTHOR INFORMATION

Corresponding Author

younan.xia@bme.gatech.edu

Present Address

[¶]The Wallace H. Coulter Depatment of Biomedical Engineering and School of Chemistry and Biochemistry, Georgia Institute of Technology, Atlanta, Georgia 30332, United States

Author Contributions

[▽]These authors contributed equally to this work.

Notes

The authors declare no competing financial interest.

■ ACKNOWLEDGMENTS

This work was supported in part by the NSF (DMR, 1104614 and 1215034) and startup funds from Washington University in St. Louis. As a jointly supervised Ph.D. student from Southeast University, C.Z. was also partially supported by a Fellowship from the China Scholarship Council. Y.X. was also partially supported by the World Class University (WCU) program through the National Research Foundation of Korea funded by the Ministry of Education, Science and Technology (R32-20031). The work at BNL was supported by the U.S. Department of Energy, Basic Energy Sciences, by the Materials Sciences and Engineering Division under Contract No. DE-AC02-98CH10886 and through the use of CFN.

■ REFERENCES

(1) Rodriguez, J. A.; Goodman, D. W. *Science* **1992**, *257*, 897.
(2) Link, S.; Wang, Z. L.; El-Sayed, M. A. *J. Phys. Chem. B* **1999**, *103*, 3529.
(3) Xia, Y.; Xiong, Y.; Lim, B.; Skrabalak, S. E. *Angew. Chem., Int. Ed.* **2009**, *48*, 60.
(4) Wang, D.; Li, Y. *Adv. Mater.* **2011**, *23*, 1044.
(5) Yang, H. *Angew. Chem., Int. Ed.* **2011**, *50*, 2674.
(6) Peng, Z.; Yang, H. *Nano Today* **2009**, *4*, 143.
(7) Tedsree, K.; Li, T.; Jones, S.; Chan, C. W. A.; Yu, K. M. K.; Bagot, P. A. J.; Marquis, E. A.; Smith, G. D. W.; Tsang, S. C. E. *Nat. Nanotechnol.* **2011**, *6*, 302.
(8) Lim, B.; Jiang, M.; Camargo, P. H. C.; Cho, E. C.; Tao, J.; Lu, X.; Zhu, Y.; Xia, Y. *Science* **2009**, *324*, 1302.
(9) Guo, S.; Sun, S. *J. Am. Chem. Soc.* **2012**, *134*, 2492.
(10) Mazumder, V.; Chi, M.; Mankin, M. N.; Liu, Y.; Metin, O.; Sun, D.; More, K. L.; Sun, S. *Nano Lett.* **2012**, *12*, 1102.
(11) Yuan, Q.; Zhou, Z.; Zhuang, J.; Wang, X. *Chem. Mater.* **2010**, *22*, 2395.
(12) Qu, Y.; Cheng, R.; Su, Q.; Duan, X. *J. Am. Chem. Soc.* **2011**, *133*, 16730.
(13) Cui, C.; Yu, J.; Li, H.; Gao, M.; Liang, H.; Yu, S. *ACS Nano* **2011**, *5*, 4211.
(14) Adams, B. D.; Wu, G.; Nigro, S.; Chen, A. *J. Am. Chem. Soc.* **2009**, *131*, 6930.
(15) Link, S.; Burda, C.; Wang, Z. L.; El-Sayed, M. A. *J. Chem. Phys.* **1999**, *111*, 1255.
(16) Zeng, J.; Zhu, C.; Tao, J.; Jin, M.; Zhang, H.; Li, Z.; Zhu, Y.; Xia, Y. *Angew. Chem., Int. Ed.* **2012**, *51*, 2354.
(17) Huang, X.; Tang, S.; Liu, B.; Ren, B.; Zheng, N. *Adv. Mater.* **2011**, *23*, 3420.
(18) Ma, Y.; Li, W.; Cho, E. C.; Li, Z.; Yu, T.; Zeng, J.; Xie, Z.; Xia, Y. *ACS Nano* **2010**, *4*, 6725.
(19) Wei, W.; Li, S.; Millstone, J. E.; Banholzer, M. J.; Chen, X.; Xu, X.; Schatz, G. C.; Mirkin, C. A. *Angew. Chem., Int. Ed.* **2009**, *48*, 4210.
(20) Kim, J.; Park, S.; Lee, J. E.; Jin, S. M.; Lee, J. H.; Lee, I. S.; Yang, I.; Kim, J.; Kim, S. K.; Cho, M.; Hyeon, T. *Angew. Chem., Int. Ed.* **2006**, *45*, 7754.
(21) Gu, H.; Yang, Z.; Gao, J.; Chang, C. K.; Xu, B. *J. Am. Chem. Soc.* **2005**, *127*, 34.
(22) Yin, A.; Min, X.; Zhang, Y.; Yan, C. *J. Am. Chem. Soc.* **2011**, *133*, 3816.
(23) Zhang, H.; Jin, M.; Wang, J.; Li, W.; Camargo, P. H. C.; Kim, M. J.; Yang, D.; Xie, Z.; Xia, Y. *J. Am. Chem. Soc.* **2011**, *133*, 6078.
(24) Sobal, N. S.; Hilgendorff, M.; Möhwald, H.; Giersig, M.; Spasova, M.; Radetic, T.; Farle, M. *Nano Lett.* **2002**, *2*, 621.
(25) Srnová-Šloufová, I.; Vlcková, B.; Bastl, Z.; Hasslett, T. L. *Langmuir* **2004**, *20*, 3407.
(26) Son, S. U.; Jang, Y.; Park, J.; Na, H. B.; Park, H. M.; Yun, H. J.; Lee, J.; Hyeon, T. *J. Am. Chem. Soc.* **2004**, *126*, 5026.
(27) McKiernan, M.; Zeng, J.; Ferdous, S.; Verhaverbeke, S.; Leschkies, K. S.; Gouk, R.; Lazik, C.; Jin, M.; Briseno, A. L.; Xia, Y. *Small* **2010**, *6*, 1927.
(28) Lee, Y. W.; Kim, M.; Kim, Z. H.; Han, S. W. *J. Am. Chem. Soc.* **2009**, *131*, 17036.
(29) Zhang, J.; Fang, J. *J. Am. Chem. Soc.* **2009**, *131*, 18543.
(30) Yang, J.; Ying, J. Y. *Nat. Mater.* **2009**, *8*, 683.
(31) Wu, J.; Gross, A.; Yang, H. *Nano Lett.* **2011**, *11*, 798.
(32) Zhang, J.; Yang, H.; Fang, J.; Zou, S. *Nano Lett.* **2010**, *10*, 638.
(33) Abbott, H. L.; Aumer, A.; Lei, Y.; Asokan, C.; Meyer, R. J.; Sterrer, M.; Shaikhutdinov, S.; Freund, H. J. *J. Phys. Chem. C* **2010**, *114*, 17099.
(34) Nikoobakht, B.; El-Sayed, M. A. *Chem. Mater.* **2003**, *15*, 1957.
(35) Jin, R.; Cao, Y. C.; Hao, E.; Metraux, G. S.; Schatz, G. C.; Mirkin, C. A. *Nature* **2003**, *425*, 487.
(36) Gole, A.; Murphy, C. J. *Chem. Mater.* **2004**, *16*, 3633.
(37) Sau, T. K.; Murphy, C. J. *J. Am. Chem. Soc.* **2004**, *126*, 8648.
(38) Bisson, L.; Boissiere, C.; Nicole, L.; Grosso, D.; Jolivet, J. P.; Thomazeau, C.; Uzio, D.; Berhault, G.; Sanchez, C. *Chem. Mater.* **2009**, *21*, 2668.
(39) Chen, Y.; Hung, H.; Huang, M. H. *J. Am. Chem. Soc.* **2009**, *131*, 9114.
(40) Berhault, G.; Bausach, M.; Bisson, L.; Becerra, L.; Thomazeau, C.; Uzio, D. *J. Phys. Chem. C* **2007**, *111*, 5915.
(41) Seo, D.; Yoo, C. I.; Jung, J.; Song, H. *J. Am. Chem. Soc.* **2008**, *130*, 2940.
(42) Feng, Y.; He, J.; Wang, H.; Tay, Y. Y.; Sun, H.; Zhu, L.; Chen, H. *J. Am. Chem. Soc.* **2012**, *134*, 2004.
(43) Wang, F.; Li, C.; Sun, L.; Wu, H.; Ming, T.; Wang, J.; Yu, J. C.; Yan, C. *J. Am. Chem. Soc.* **2011**, *133*, 1106.
(44) Habas, S. E.; Lee, H.; Radmilovic, V.; Somorjai, G. A.; Yang, P. *Nat. Mater.* **2007**, *6*, 692.
(45) Lu, C.; Prasad, K. S.; Wu, H.; Ho, J. A.; Huang, M. H. *J. Am. Chem. Soc.* **2010**, *132*, 14546.
(46) Fan, F.; Liu, D.; Wu, Y.; Duan, S.; Xie, Z.; Jiang, Z.; Tian, Z. *J. Am. Chem. Soc.* **2008**, *130*, 6949.
(47) Sanedrin, R. G.; Georganopoulou, D. G.; Park, S.; Mirkin, C. A. *Adv. Mater.* **2005**, *17*, 1027.

(48) Tao, A.; Sinsermsuksakul, P.; Yang, P. *Angew. Chem., Int. Ed.* **2006**, *45*, 4597.
(49) Li, J.; Zheng, Y.; Zeng, J.; Xia, Y. *Chem.—Eur. J.* **2012**, *18*, 8150.
(50) Suito, E.; Uyeda, N. *Nature* **1960**, *185*, 453.
(51) Jin, M.; Liu, H.; Zhang, H.; Xie, Z.; Liu, J.; Xia, Y. *Nano Res.* **2011**, *4*, 83.
(52) Jin, M.; Zhang, H.; Xie, Z.; Xia, Y. *Energy Environ. Sci.* **2012**, *5*, 6352.
(53) Zhang, Q.; Ge, J.; Pham, T.; Goebl, J.; Hu, Y.; Lu, Z.; Yin, Y. *Angew. Chem., Int. Ed.* **2009**, *48*, 3516.
(54) Zeng, J.; Roberts, S.; Xia, Y. *Chem.—Eur. J.* **2010**, *16*, 12559.
(55) Zeng, J.; Tao, J.; Su, D.; Zhu, Y.; Qin, D.; Xia, Y. *Nano Lett.* **2011**, *11*, 3010.
(56) Pietrobon, B.; Kitaev, V. *Chem. Mater.* **2008**, *20*, 5186.
(57) Pietrobon, B.; McEachran, M.; Kitaev, V. *ACS Nano* **2009**, *3*, 21.
(58) Haynes, C. L.; McFarland, A. D.; Van Duyne, R. P. *Anal. Chem.* **2005**, *77*, 338A.
(59) Willets, K. A.; Van Duyne, R. P. *Annu. Rev. Phys. Chem.* **2007**, *58*, 267.
(60) Haes, A. J.; Haynes, C. L.; McFarland, A. D.; Schatz, G. C.; Van Duyne, R. P.; Zou, S. *MRS Bull.* **2005**, *30*, 368.
(61) Lide, D. R. *CRC Handbook of Chemistry and Physics*, 88th ed.; CRC Press/Taylor and Francis: Boca Raton, FL, 2008.
(62) Xia, X.; Zeng, J.; Oetjen, L. K.; Li, Q.; Xia, Y. *J. Am. Chem. Soc.* **2012**, *134*, 1793.
(63) Zhou, J.; Zeng, J.; Grant, J.; Wu, H.; Xia, Y. *Small* **2011**, *7*, 3308.
(64) Skoog, D. A.; West, D. M.; Holler, F. J. *Fundamentals of Analytical Chemistry*, 7th ed.; Sauders College Publishing: Philadelphia, PA, 1996; Appendix 5